

Reaction kinetics of hydrogen-gold complexes in silicon

Einar Ö. Sveinbjörnsson and Olof Engström

Department of Solid State Electronics, Chalmers University of Technology, S-412 96 Göteborg, Sweden

(Received 5 December 1994; revised manuscript received 23 March 1995)

We report studies of hydrogen-gold (Au-H) complexes in gold-doped silicon formed after hydrogen injection during wet chemical etching. Using deep-level transient spectroscopy we find three deep levels that most likely belong to the same Au-H center, labeled *G*. This electrically active Au-H center transforms irreversibly into an electrically inactive Au-H complex during annealing at temperatures above 150°C. This transformation seems to occur only when excess atomic hydrogen is present in the sample in the vicinity of the Au-H complexes. Based on the annealing kinetics we tentatively assign the active complex to a Au-H pair and the passive one to Au-H₂.

I. INTRODUCTION

Hydrogen in crystalline silicon has been studied extensively during the past decade.^{1,2} The element is inevitably introduced into silicon during device processing, for example during wafer polishing, wet or dry etching, ion implantation, sputtering of contact metals, or even during boiling in water.³ Considerable progress has recently been made in understanding the properties of isolated atomic hydrogen in silicon. Apparently, it is a negative-*U* center with a single donor level located about 0.2 eV below the conduction band,⁴⁻⁶ and an acceptor level close to the middle of the band gap.⁷ Also, complexes between hydrogen and shallow dopant impurities are reasonably well understood.² However, in the case of the interaction between hydrogen and deep-level metallic impurities the picture is less clear. Most experimental investigations find that if hydrogen interacts with the deep-level defect the electrical activity of the deep center is removed from the silicon band gap.⁸ The structure of such hydrogen-deep-level-defect complexes has rarely been investigated with spectroscopic techniques, the main reason being the limited penetration depth of atomic hydrogen in silicon when introduced by remote hydrogen plasma.³

It has recently been recognized that a uniform hydrogen density in the 10^{15}-cm^{-3} range can be achieved in silicon by annealing in molecular hydrogen ambient at very high temperature, typically 1200–1300°C.^{9,10} This hydrogenation technique has enabled spectroscopic studies of hydrogen-platinum complexes.^{11,12} The Pt-H₂ complex is electrically active with a shallow level that could have been missed in previous studies using deep-level transient spectroscopy (DLTS).^{11,13} Recently a number of deep levels related to hydrogen and transition-metal impurities have been reported.¹⁴⁻¹⁹ These levels are unstable above $\approx 200^\circ\text{C}$ and are generally not observed if hydrogen is introduced into the silicon in this temperature range.

Hydrogen passivation of the gold center^{20,21} in silicon was first reported by Pearton and Tavendale using remote plasma hydrogenation.²² The actual kinetics of the gold passivation have not been properly examined. Recently

we reported hydrogen-gold-related deep levels in *n*- and *p*-type silicon after hydrogen injection by wet chemical etching.^{14,16,17} The levels were attributed to electrically active Au-H complexes that transformed into electrically inactive Au-H configurations during annealing at $\approx 150^\circ\text{C}$.

The present paper comprises our studies of these Au-H complexes. Before presenting the details we find it appropriate to summarize our findings in one schematic diagram. Figure 1 shows all the reactions observed involving gold and hydrogen. For historical reasons the notation is somewhat complicated, but we claim that we find three deep levels *G*1, *G*2, and *G*4 of the *same* Au-H complex. This Au-H complex is labeled *G*. Another Au-H complex, PA (passive), has no deep levels within the band gap. In the text below we first demonstrate that the complexes observed are related to hydrogen and gold. Thereafter we present experimental data that support the reactions depicted in Fig. 1.

II. EXPERIMENT

The starting material was 2 and 3-in. floating zone (FZ) or Czochralski grown (CZ), (100)-oriented *p*-type (boron)

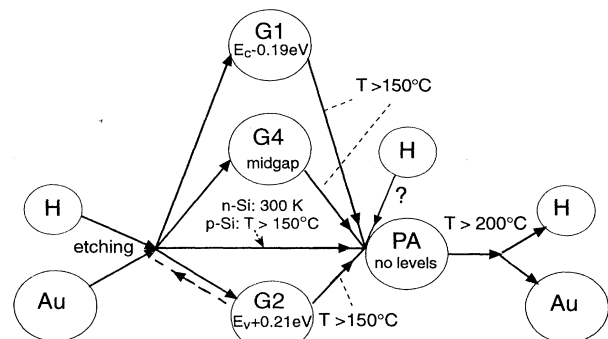


FIG. 1. Schematic diagram of the reactions observed involving gold and hydrogen. The *G* levels *G*1, *G*2, and *G*4 appear after etching. The deep levels disappear during annealing at 150°C and a passive Au-H complex is formed (PA). Apparently additional hydrogen is needed for this process to occur. A part of the gold in *n*-type samples is already passivated at room temperature as inactive Au-H complexes, PA.

and *n*-type (phosphorus) silicon wafers with resistivities in the range 1–70 Ω cm. The formation and annealing kinetics of the Au-H complexes were independent of the substrate used. Details of the gold doping procedure have been given elsewhere.²³ The wafers were coated with an approximately 1500-Å-thick gold layer on one side. The gold was driven in at temperatures between 800 and 900°C, in nitrogen ambient, for several hours depending on the substrate used. The diffusion times and temperatures were such that the resulting gold concentration was about 10% of the shallow doping concentration. The gold profile after diffusion was *U* shaped, but uniform gold doping was achieved after etching about 50 μ m off the water surfaces using isotropic silicon etch (HNO_3 : HF: CH_3COOH : HClO_4 , 7.3:2.9:2:1).²³

Schottky contacts on *p*-type samples were formed by evaporation or sputtering of aluminum or titanium at room temperature. Gold or aluminum layers were evaporated onto *n*-type samples to achieve Schottky diodes. A GaAl alloy was rubbed onto the reverse sides of the *n*-type samples for Ohmic contacts. Gold or GaAl was used as Ohmic contacts on *p*-type samples. No deep levels were detected with deep-level transient spectroscopy (DLTS) in reference samples not doped with gold.

The Schottky diodes were characterized using DLTS and high-frequency (1 MHz) capacitance-voltage (*CV*) profiling. The details of the experimental setup have been given elsewhere.²⁴ The depth profiles of the deep traps were obtained by capacitance DLTS depth profiling. The profiles were corrected for the nonuniform shallow doping profile because of hydrogen passivation of dopants. This effect is more pronounced in boron-doped material, but the features observed in this work are easily resolved assuming uniform shallow doping concentrations. The majority-carrier capture cross sections were measured by conventional pulse-filling techniques.²⁵ Heat treatments at temperatures $\leq 130^\circ\text{C}$ were performed in the dark inside the cryostat in helium ambient. Otherwise the samples were annealed in a diffusion furnace in nitrogen ambient. The Schottky diodes were sensitive to heat treatments above 150°C and degraded frequently during such annealing. This is a major drawback when studying the dissociation of the hydrogen-gold complexes that becomes appreciable at $\approx 200^\circ\text{C}$. The quality of the diodes after each annealing was studied by *CV* profiling and current-voltage measurements.

III. RESULTS

A. Formation of electrically active Au-H complexes in *p*-type Si by reverse bias annealing

In a previous paper¹⁶ we demonstrated that etching of *p*-type Si results in diffusion of hydrogen into the sample surface layer (depth less than 2 μ m) where deactivation of boron acceptors occurs. From a series of reverse bias annealing (RBA) experiments we found that the reactivation rates of boron dopants agreed with the annealing kinetics of boron-hydrogen complexes reported in the literature.²⁶ The involvement of hydrogen in the *p*-type samples is therefore evident. However, most importantly

we also demonstrate a strong correlation between the profiles of the deep traps and the distribution of hydrogen in the samples.

Figure 2(a) shows typical DLTS spectra of *p*-type gold-doped samples. Curve 1 is the initial spectrum after etching and evaporation of an aluminum Schottky contact. Spectrum 2 was recorded after reverse bias annealing (RBA) at 120°C for 10 min using a bias of -3 V. A total of five DLTS peaks are observed. The small peak at approximately 180 K is occasionally detected in gold-doped samples, and has not been identified while all other signals are consistently observed after gold doping and etching. The activation energies of the peaks and their hole capture cross sections are summarized in Table I together with previous data on *n*-type samples.¹⁴ The peak at approximately 160 K is attributed to the gold donor with an activation energy of 0.35 eV (using T^2 adjustment). The broad peak at approximately 280 K has an activation energy of ≈ 0.53 eV. A similar signal has previously been reported in *p*-type gold-doped Schottky diodes and attributed to non-negligible hole emission from the gold acceptor level.²⁷ This agrees with our studies of samples having different gold concentrations. We observed that the peak height of the signal at ≈ 280 K was correlated with the gold donor concentration.

Reverse bias annealing had an effect on the four main DLTS peaks (curve 2). *G2* and *G3* were enhanced after RBA while the gold donor signal decreased and the Au acceptor peak at 280 K was shifted toward higher temperatures. This shift of the Au acceptor peak is due to an

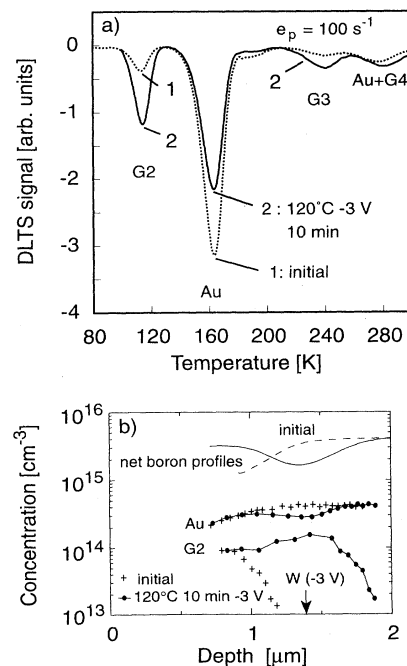


FIG. 2. (a) DLTS spectra of a *p*-type gold-doped sample before (1) and after (2) reverse bias annealing (RBA) for 10 min using -3 -V bias. (b) Concentration depth profiles of *G2*, gold donors, and boron before and after the RBA. The depletion layer edge *W* during the annealing is also indicated.

TABLE I. Activation energies ΔE (using T^2 adjustment) and majority-carrier capture cross sections σ_p or σ_n of the deep levels in p - and n -type samples. No temperature dependence of the cross sections was observed within the temperature range indicated.

Peak	ΔE (eV)	σ_p (cm ²)	σ_n (cm ²)	T (K)
G2	0.21	1.7×10^{-15}		100–125
Au ^{0/+}	0.35	1.0×10^{-15}		150–180
G3	0.47	5×10^{-16}		228–250
Au ⁻⁰ +G4	≈ 0.53			
G1	0.19		1×10^{-17}	90–120
Au ⁻⁰ +G4	0.56		1×10^{-16}	260–300

additional signal, G4, that is correlated with the G2 signal. We will return to this shift in Sec. III E. The effect of the reverse bias annealing illustrated by curve 2 was observed in all p -type substrates.

The purpose of the reverse bias heat treatment was to drive the atomic hydrogen from the surface layer deeper into the bulk. We monitored this by studying the active boron acceptor depth profiles from capacitance voltage (CV) analysis before and after RBA. Figure 2(b) shows the corresponding depth profiles of active boron acceptors, gold donors, and G2 before and after RBA. The depletion layer edge during RBA was at approximately 1.4 μm . We note the correlation of the trap profiles and the active boron profile. During the heat treatment B-H pairs dissociated. The released positively charged atomic hydrogen was driven toward the depletion layer edge where three processes occurred: (1) additional B-H pairs formed, (2) the active gold donor density decreased, and (3) the G2 concentration increased by roughly the same amount. We observed earlier that all these changes followed the depletion layer edge, and that the profiles can be modulated by adjusting the reverse bias.¹⁶ Furthermore, no significant changes in the trap profiles were observed if the samples were annealed under a reverse bias at lower temperatures where the B-H pairs are stable. This demonstrates that the B-H pairs act as sources of hydrogen, and that the G2 trap is evidently hydrogen related. No passivation of gold donors was observed at this temperature, i.e., the G2 concentration fully accounted for the decrease of the gold donor concentration. This was no longer true if the temperature was raised to 150 °C, as demonstrated below.

B. Formation of electrically inactive Au-H complexes in p -Si at 150 °C

Figure 3(a) shows the concentrations of G2 and gold donors as functions of annealing time at 150 °C without bias. The sample was first annealed as in Fig. 2. The trap concentrations were estimated with DLTS between depths of ≈ 1.1 – $1.6 \mu\text{m}$ (reverse bias 5 V, filling pulse 4 V). During the first 10 min the G2 concentration increased while the gold donor concentration steadily decreased. Thereafter concentrations of both traps decreased. This was not accompanied by any additional DLTS peaks; the gold involved was apparently passivated. We label the passive hydrogen-gold complex PA.

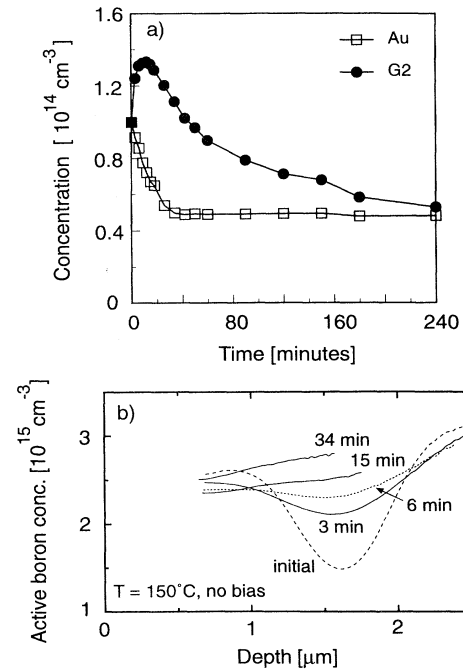


FIG. 3. Connection between B-H dissociation and formation of Au-H complexes. (a) Concentrations of G2 and gold donors as functions of time at 150 °C. (b) Simultaneous dissociation of B-H pairs at 150 °C estimated by CV profiling. Most of the B-H pairs dissociate during the first 30 min, and no significant change is observed in the net boron profiles upon further annealing.

The gold donor density became stable after about 30 min, and remained unchanged during further annealing. The electrically inactive gold centers remained passivated unless the sample temperature was raised above 150 °C.

Figure 3(b) shows the simultaneous reactivation of boron acceptors. Most of the B-H complexes were dissociated after about 30-min annealing, and no significant change was seen in the active boron acceptor density upon further annealing (not shown). Again, the B-H pairs clearly acted as sources of atomic hydrogen to form Au-H complexes. The gold donor density [Fig. 3(a)] became constant at the same time as most of the B-H pairs dissociated. A reverse bias annealing treatment at 120 °C of a similar sample revealed that the remaining B-H density after 60-min zero bias annealing at 150 °C was approximately $5 \times 10^{14} \text{ cm}^{-3}$ in the region where DLTS data were collected (at depths between 1.1 and 1.6 μm).

The reactions in Fig. 3(a) are interpreted as follows. During the first 10-min hydrogen released from B-H pairs formed both electrically active (G2) and inactive (PA) complexes with gold. Then during the next 20 min or so the Au \rightarrow PA reaction still occurred while there was a net transformation of G2 complexes into PA complexes (G2 \rightarrow PA). This was the only transition observed during further annealing.

C. Annealing kinetics during reverse bias annealing at 150 °C

The reactions depicted in Fig. 3 depend strongly on the availability of hydrogen in the sample. This is shown in

Fig. 4. The sample was first preannealed at 120°C for 10 min using -3 -V bias to inject hydrogen and form $G2$. Then the sample was annealed at 120°C for 10 min using -3 -V bias to inject hydrogen and form $G2$. Then the sample was annealed at 120°C for 60 min using a reverse bias of -15 V. During the first 15 min, at -15 -V bias, hydrogen released from B-H pairs was driven toward the depletion layer edge at ≈ 2.5 μm , where additional B-H complexes were formed. This is seen as a decrease in the active boron density profile in Fig. 4(a) at ≈ 2.5 μm . Further RBA (30- and 60-min curves) resulted in negligible changes in the active boron density at depths less than 1.5 μm , demonstrating that virtually all B-H pairs have dissociated in this region. The concentrations of gold donors $G2$ and $G3$ at depths between 0.9 and 1.4 μm did not change significantly during the RBA treatment.

Figure 4(b) shows the changes in the densities of $G2$, $G3$, and gold donors during annealing at 150°C using a reverse bias of -15 V. The sample was first preannealed as shown in Fig. 4(a). The annealing kinetics are completely different from those observed in Fig. 3(a). As expected, no gold donor passivation was observed. In contrast, the gold donor concentration increased with annealing time. The increase of the gold donor density

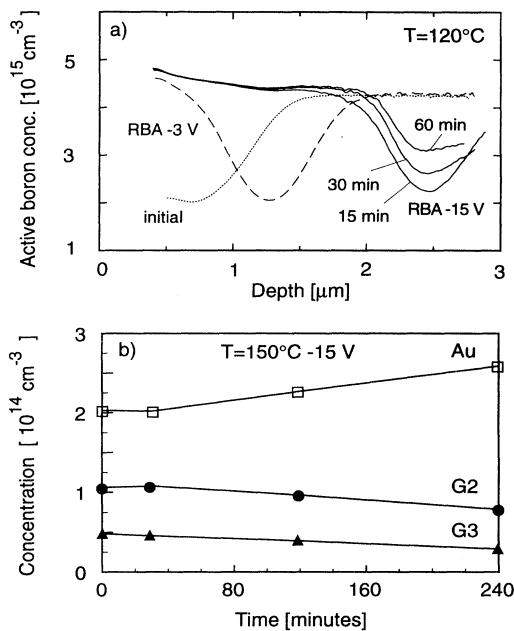


FIG. 4. Annealing kinetics of Au-H complexes when no excess hydrogen was present in the surroundings. (a) Active boron concentration in a sample during preannealing at 120°C. First, hydrogen was injected by RBA (-3 V) for 10 min to form the Au-H complexes ($G2$). This resulted in a dip of the boron profile close to the depletion layer edge at ≈ 1.4 μm because of B-H pairing. Thereafter the sample was annealed using -15 -V bias for 60 min to remove virtually all B-H complexes at depths between 0.9 and 1.4 μm where the deep-level concentrations were estimated using DLTS. (b) Concentrations of the deep levels in the sample during RBA (-15 V) at 150°C. The sample was first preannealed as shown in (a).

roughly equaled the simultaneous decrease of the concentrations of $G2$ and $G3$ centers. Apparently, the $G2$ complexes dissociated during the annealing instead of transforming into passive Au-H complexes as in Fig. 3(a). This suggests that excess hydrogen is needed to transform $G2$ into PA complexes. In other words PA contains more hydrogen atoms than $G2$.

Similar annealing kinetics were observed if no bias was applied to a sample during annealing at 150°C, provided that virtually all B-H pairs in the region monitored with DLTS had been removed by preannealing at 120°C using a -15 -V bias. This demonstrates that the reactions depend on the availability of hydrogen rather than the bias applied during annealing.

D. Reversible transitions between the $G2$ level and the gold donor level

The annealing behavior of $G2$ at lower temperatures also depends on the availability of hydrogen in the surroundings. This is shown in Fig. 5. The sample was first processed as the sample in Fig. 3, except that the duration of the heat treatment at 150°C was 60 min. Thereafter the sample was annealed repeatedly at 100°C without bias. Figure 4(a) shows that during the annealing the $G2$ peak decreased while the gold donor peak increased by

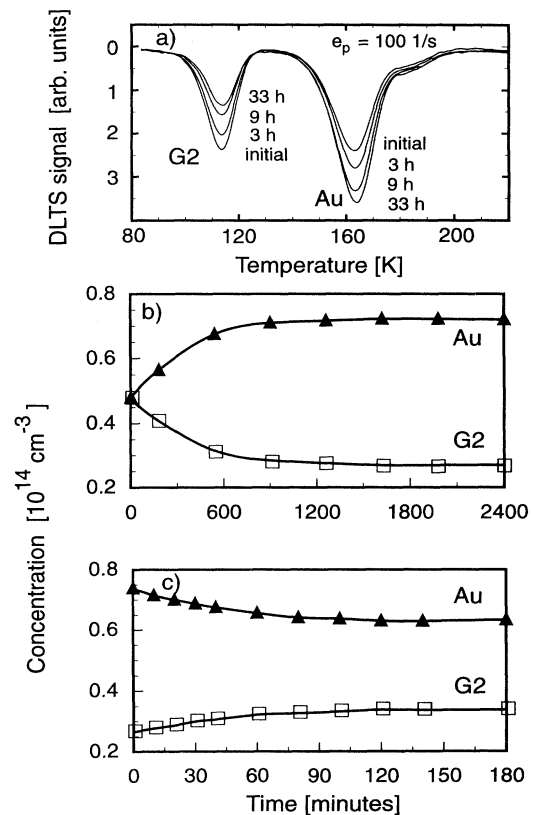


FIG. 5. (a) DLTS spectra of p -Si showing the transformation of $G2$ traps into gold donors at 100°C. (b) Concentrations of gold donors and $G2$ vs annealing time at 100°C. (c) Gold donors and $G2$ densities during annealing at 120°C starting from equilibrium at 100°C.

the same amount. After ≈ 20 h an equilibrium was reached as illustrated in Fig. 5(b). The reaction was reversed by annealing the sample further at 120°C as shown in Fig. 5(c). We found that this process was fully reversible when the sample was annealed repeatedly at temperatures between 75 and 130°C . No significant changes were observed in the active boron profiles during these annealing cycles, but reverse bias annealing at the end of the experiment revealed that the concentration of B-H pairs was approximately $5 \times 10^{14} \text{ cm}^{-3}$ in the region monitored by DLTS.

The reactions depicted in Fig. 5 were fully terminated if reverse bias was applied to the sample for times long enough to dissociate virtually all B-H pairs, and drive the released hydrogen deeper into the sample. After such treatment (120°C , 60 min, -15-V bias) no change was observed in $G2$ and Au donor peaks during annealing (with or without bias) using annealing times up to 100 times longer than needed to reach equilibrium in Figs. 5(b) and 5(c).

The simplest explanation of the data in Fig. 5 is that depending on the annealing temperature there is a net dissociation or association of $G2$ with the excess hydrogen stored in B-H complexes. Still we point out the remarkable feature that $G2$ dissociates much faster when free hydrogen is available in the surroundings, since $G2$ became stable when excess hydrogen was removed by RBA. For example, the dissociation rate of $G2$ at 100°C in Fig. 5(b) is higher than at 150°C in the hydrogen-free environment shown in Fig. 4(b). We will return to this in Sec. IV.

E. Connection between DLTS peaks in p -type Si

As mentioned above, the gold acceptor peak in Fig. 2(a) was shifted towards higher temperatures after the heat treatment. This shift is correlated with the $G2$ peak as demonstrated in Fig. 6. The figure shows DLTS spectra of a p -type sample after several successive heat treatments. Curve a is the initial spectrum after etching. Curve b is after injection of hydrogen by RBA for 10 min at 120°C followed by annealing for 60 min at 150°C . The $G2$ signal was then stronger than the gold donor signal, and we note the shift of the gold acceptor peak. Curve c is after further annealing at 100°C for 24 h. As in Fig. 5(a), the $G2$ peak decreased during the annealing, and the gold donor peak increased correspondingly. Also, the gold acceptor peak was shifted to lower temperatures. This correlation between $G2$ and the shift of the gold acceptor peak is always observed. We attribute this shift to emission from a deep level $G4$ close by in energy to the gold acceptor level. The data suggest that $G2$ and $G4$ belong to the same Au-H complex.

Figure 6 shows that the $G3$ signal annealed out irreversibly during the heat treatment at 100°C (curve c). $G3$ was enhanced after reverse bias annealing as shown by curve 2 in Fig. 2, and the $G3$ enhancement followed the depletion layer edge in a similar way as $G2$ did.¹⁶ The $G3$ signal is therefore clearly hydrogen related. However, the annealing behavior differs from that of $G2$, as shown in Fig. 6. Therefore, it is probable that $G3$ does not originate from the same hydrogen-gold complex as $G2$.

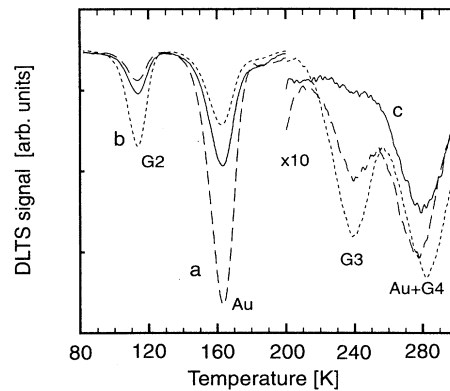


FIG. 6. DLTS spectra of p -Si showing the shift in the gold acceptor peak at ≈ 280 K (curve a). Initial spectrum after etching (curve b) after reverse bias annealing for 10 min at 120°C (-3-V bias) followed by heat treatment at 150°C for 60 min, and (curve c) after additional heat treatment for 24 h at 100°C . The shift of the gold acceptor peak is connected to the intensity of the $G2$ signal and is attributed to a new deep level $G4$ close to the gold acceptor level. The $G3$ level annealed out during the heat treatment at 100°C .

F. Formation of $G1$ and temperature shift of the gold acceptor peak in n -Si

Recently we reported^{14,17} that etching n -type gold-doped silicon gives rise to a deep level $G1$ in the sample surface region. In addition, passivation of gold acceptors and phosphorus dopants was observed closest to the surface. From the reactivation kinetics of phosphorus donors it was deduced that the deactivation of phosphorus was due to phosphorus-hydrogen (P-H) pairs.¹⁷ The $G1$ level was attributed to a hydrogen-gold complex. The thermal stability of the P-H pairs is poor, and most of them may even dissociate during deposition of the Schottky contact if the sample temperature exceeds room temperature. If this occurs there are no electrical signs of hydrogen in the samples. This was indeed the case in some of the samples that were coated with aluminum. Also, only part of the hydrogen-injected forms pairs with the phosphorus dopants. Therefore it was not possible to trace the concentration of atomic hydrogen with CV profiling as in p -type samples.

Curve 1 in Fig. 7(a) is a typical DLTS spectrum of a gold-doped n -type sample after etching. Two peaks are observed, Au+ $G4$ at ≈ 273 K, and $G1$ at ≈ 110 K. Below we will demonstrate that the Au+ $G4$ peak is a mixture of electron emission from the gold acceptor level and electron emission from a hydrogen-gold-related deep level. Curve 2 was taken after 30-min annealing at 250°C . The $G1$ signal annealed out at the same time as the Au+ $G4$ peak increased and shifted toward higher temperatures. This shift is consistently observed but only when detecting electron emission in the hydrogenated surface region. No shift of the Au+ $G4$ peak is observed when emission from centers beneath the hydrogenated region is monitored before and after etching. The shift is largest when comparing emission from traps within the surface region, where deactivation of phosphorus occurs

and *G1* is formed, and emission from traps in the region beneath the hydrogenated region. This is demonstrated in Fig. 7(b). Using biases between 0- and -2-V emission from traps within the hydrogenated region (depths 1–2 μm) was monitored as shown in curve 1. Curve 2 is the spectrum when biasing between -5 and -10 V. Then emission is detected from traps in a region virtually free of hydrogen, at depths between 2.5 and 3.5 μm . Arrhenius plots of the electron emission rates in these two cases are shown in Fig. 7(c). The difference between the rates in the two regions is more or less independent of

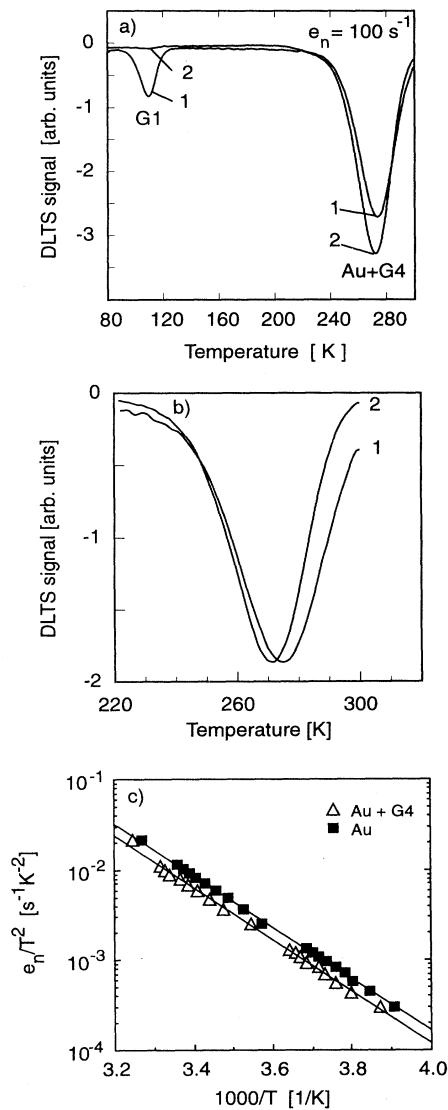


FIG. 7. (a) Curve 1, DLTS spectrum of *n*-type gold-doped Si after etching. Curve 2 is after 30-min heat treatment at 250°C. (b) Two DLTS spectra demonstrating the shift of the gold acceptor peak after etching. Curve 1 was recorded in the hydrogenated region; reverse bias 2 V, filling pulse 2 V. Curve 2 was recorded beneath the hydrogenated region; reverse bias 10 V, filling pulse 5 V. The shift is attributed to a hydrogen-gold-related deep level *G4*. (c) Arrhenius plot of the electron emission rates estimated in the two regions monitored in (b).

temperature, and we obtained an activation energy of ≈ 0.56 eV in both cases. This suggests that the shift is due to a difference in the prefactors, i.e., the electron-capture cross sections or the entropy factors of the exponential function determining the graphs in Fig. 7(c).²⁸ The difference between the prefactors is about 20%. We have estimated the electron-capture rates c_n using pulse-filling experiments,²⁵ and obtained the same electron-capture cross section $\sigma_n \approx 1.0 \times 10^{-16}$ cm² for both centers. The uncertainty in this value is larger than 20%. It is therefore not possible to resolve whether the differences in the electron emission rates are due to differences in the capture cross sections or the entropy factors of the two levels.

The data in Fig. 7 suggest that the Au+*G4* peak in hydrogenated samples consists of two contributions, one from isolated gold acceptors and the other from a hydrogen-gold-related center. A similar shift of the gold acceptor peak was observed in *p*-type material (see Sec. III E, Fig. 6) where it was attributed to a deep level labeled *G4*. This suggests that the shifts observed in *p*- and *n*-type samples are due to the same hydrogen-gold-related deep level, namely *G4*. Also, the concentration depth profiles of the deep traps shown below support this picture.

Figure 8 shows the annealing behavior of *G1* and Au+*G4* in three identically prepared *n*-type samples (I, II, and III). The initial profiles in Fig. 8(a) (filled trian-

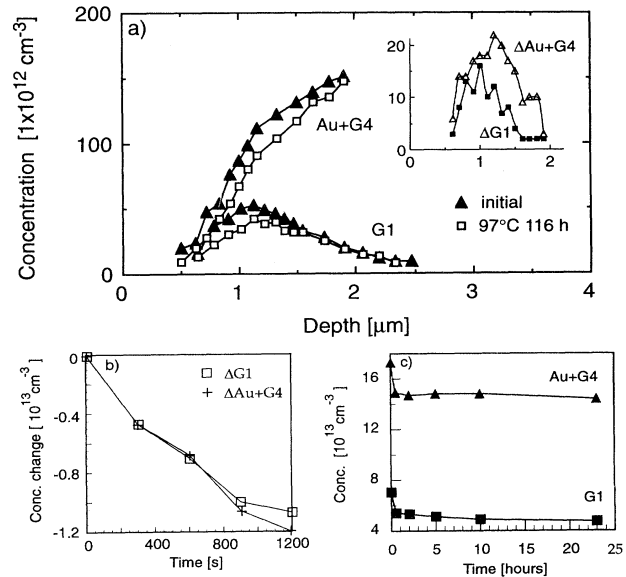


FIG. 8. Concentrations of *G1* and Au+*G4* in three identically prepared *N*-type samples. (a) Depth profiles of *G1* and (Au+*G4*) in sample I. Filled triangles are the profiles after etching followed by heat treatment at 97°C, for 24 h. Empty squares denote the profiles after additional heat treatment for 116 h at 97°C. The inset shows the decrease of both profiles due to the heat treatment. (b) Changes in the *G1* and (Au+*G4*) concentrations in the surface region (0.5–1.5 μm) of sample II during successive heat treatments at 150°C. (c) *G1* and (Au+*G4*) concentrations in sample III as functions of annealing time at 150°C.

gles) of sample I were after etching followed by reverse bias annealing (10 V) for 24 h at 97°C. These profiles are reproducible from sample to sample and are observed in four different *n*-type substrates (FZ and CZ grown). The purpose of the heat treatment was to dissociate all phosphorus-hydrogen pairs. This preannealing had only a minor effect on the depth profiles of *G*1 and Au+*G*4 (not shown). The *G*1 concentration is negligible at 0.5 μm, increases inward with a maximum at about 1.6 μm, decreases again deeper into the sample, and is below the detection limit ($1 \times 10^{12} \text{ cm}^{-3}$) at depths greater than 2.5 μm. The position of the maximum of the *G*1 profile is always close to the depletion layer edge.¹⁴

Even though quantitative comparisons of the depth profiles in Fig. 8(a) are questionable, there are some features that need to be pointed out. In analogy with the Au+*G*4 peak shift in Fig. 7(b) we suggest that in the surface region the gold acceptor profile consists of two contributions, electron emission from gold acceptors and electron emission from *G*4. The Au+*G*4 profile decreases dramatically toward the sample surface and follows the *G*1 profile closely. Further, the *G*1 concentration never exceeds the Au+*G*4 concentration at any depth. This was the case in all samples investigated, both after etching and after heat treatments. The form of the initial (Au+*G*4) profile (filled triangles) in Fig. 8(a) also raises some questions. There is a shoulder in the profile at $\approx 1 \mu\text{m}$, at the same depth as the maximum of the *G*1 profile. This correlation of the depth profiles suggests that the deep levels *G*1 and *G*4 are two levels of the same Au-H complex. Closest to the surface, where the Au+*G*4 and *G*1 profiles match, virtually all gold acceptors complex with hydrogen, either as passive complexes PA, or electrically active complexes detected as *G*1 and *G*4. If this is the case, the actual gold acceptor profile is obtained by subtracting the *G*1 profile from the Au+*G*4 profile.

The profiles marked by empty squares in Fig. 8(a) were obtained after reverse bias annealing (-10 V) at 97°C for 116 h. We note that both profiles moved inwards after the annealing. The inset in the figure shows the change in the concentration profiles. The decrease of the Au+*G*4 concentration was somewhat larger than that of *G*1.

Practically the same observation was made when the concentrations of *G*1 and Au+*G*4 were monitored after successive 5-min annealings at 150°C, as shown in Fig. 8(b). The sample (II) was first preannealed at 120°C for 10 min using -10-V bias to dissociate P-H pairs. The concentrations were estimated by detection of electron emission from traps in the hydrogenated region 0.5–1.5 μm (reverse bias 2 V, filling pulse 2 V). The initial concentrations were $N_{\text{Au}+\text{G}4} = 6.2 \times 10^{13} \text{ cm}^{-3}$ and $N_{\text{G}1} = 3.0 \times 10^{13} \text{ cm}^{-3}$. We note that the concentration changes of *G*1 and Au+*G*4 were more or less equal after each heat treatment. Such behavior is expected if the electrically active Au-H complex, with its two deep levels *G*1 and *G*4, transforms into an electrically inactive Au-H complex PA.

Figure 8(c) shows the effect of longer annealing periods at 150°C on *G*1 and Au+*G*4 concentrations. The sam-

ple (III) in this study was preannealed in the same way as sample II. Both concentrations decreased during the first 30–60 min at 150°C. Thereafter no significant change was observed.

Finally, the annealing behavior of *G*1 and the Au+*G*4 depth profiles were not sensitive to reverse bias. No significant changes were observed if a reverse bias was applied to the Schottky diode during annealing at 150°C.

IV. DISCUSSION

We begin this section by briefly summarizing the main results of this work.

(i) Two hydrogen-gold-related deep levels *G*2 and *G*3 are observed in *p*-type samples after etching. The levels do not belong to the same Au-H complex (Figs. 2 and 6).

(ii) The annealing kinetics of the *G*2 signal in *p*-Si depend strongly on the concentration of free-atomic hydrogen in the immediate surroundings. If excess hydrogen is present, *G*2 can transform into an electrically inactive Au-H complex (PA) during annealing at temperatures at or above 150°C (see Sec. III B). Similarly, at lower annealing temperatures *G*2 dissociates ($\text{G}2 \rightarrow \text{Au}$) much faster in the presence of excess hydrogen (see Sec. III D).

(iii) A DLTS peak due to non-negligible hole emission from the gold acceptor level is observed in *p*-type samples. The peak is shifted to higher temperatures in the hydrogenated surface regions of the samples (Figs. 2 and 6). This shift appears in conjunction with the *G*2 signal. It is explained as follows: The gold acceptor signal is a combination of hole emission from isolated gold centers and emission from a deep level *G*4 of a Au-H complex. The correlation between *G*2 and *G*4 indicates that they are two levels of the same Au-H complex.

(iv) A Au-H-related deep level *G*1 is observed in *n*-type samples after etching. The appearance of *G*1 is correlated with a temperature shift of the gold acceptor DLTS peak (Fig. 7). The temperature shift is explained as in *p*-type samples: The gold acceptor peak consists of two contributions, one from isolated gold centers and another from *G*4. Concentration depth profiles of *G*1 and Au+*G*4 are strikingly similar in the sample surface region (Figs. 8). This together with the annealing kinetics at 150°C [Figs. 8(b) and 8(c)] indicates that *G*1 and *G*4 are two levels of the same Au-H center.

(v) The data in *p*- and *n*-type samples combined suggest that the three deep levels *G*1, *G*2, and *G*4 belong to the same Au-H complex.

A. Annealing kinetics of Au-H complexes in *p*-Si

The annealing data in Figs. 3–5 show the complexity of the reactions between gold and hydrogen. Still, it is possible to extract some useful information from the data. First is the striking behavior of the *G*2 complex which depends on whether or not there is hydrogen available to react with the complex. A remarkable feature is that *G*2 dissociates faster in the presence of hydrogen. Further, at 150°C, *G*2 transforms irreversibly into the passive Au-H complex (PA) only when atomic hydrogen is available [compare Figs. 3(a) and 4(b)]. Otherwise, *G*2

dissociates slowly at this temperature ($G2 \rightarrow Au$). This observation suggests that PA and $G2$ are two *different* Au-H complexes, and that PA contains more hydrogen atoms than $G2$. We tentatively assign $G2$ to a Au-H pair and PA to a Au- H_2 complex. We start by discussing the dissociation and association of $G2$ at low temperatures where PA complexes are not involved.

We analyzed the association and dissociation data of $G2$ in the presence of hydrogen ($[BH] \approx 5 \times 10^{14} \text{ cm}^{-3}$), and found that the data for the sample in Fig. 5 were best described by competitive first-order reactions given by

$$d[G2]/dt = k_A[Au] - k_D[G2], \quad (1)$$

where k_A and k_D are the association and dissociation rates of $G2$. The reaction rates were determined from a series of heat treatments between 75 and 130 °C following the concentration transients at each temperature. A solution of the form $k = k_0 \exp(-\Delta E/k_B T)$ was sought, where k_0 is a preexponential factor and ΔE is the activation energy for the reaction. An Arrhenius plot of the reaction rates is shown in Fig. 9. The activation energies and the prefactors extracted using a least-square fit are shown in Table II. Below we discuss possible reactions that could serve as an explanation for the experimental data in Fig. 9. We neglect possible effects of different charge states of the species involved since we have no experimental evidence yet for such dependence. Indeed, the $G2$ level appears when both species are expected to be positively charged Au^+ and H^+ , although the complex electronic properties of atomic hydrogen⁷ might influence this simple picture. The crude approach below only considers possible chemical reactions between Au and H but is able to account qualitatively for the data in Fig. 9.

Assuming that the $G2$ complex consists of one H atom and one Au atom, the simplest reaction is



If the kinetics are first order in each of the reactants, the rate equation for (2) is

$$d[AuH]/dt = k_1[H][Au] - k_2[AuH], \quad (3)$$

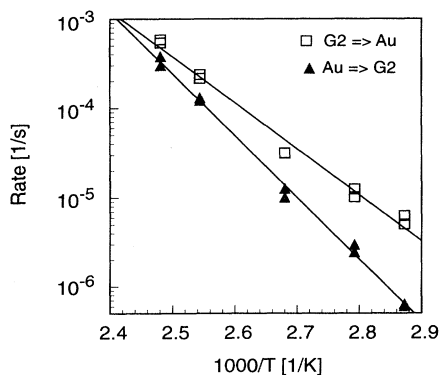


FIG. 9. Arrhenius plot of the association (triangles) and dissociation rates (squares) of the $G2$ complex extracted from concentration changes of the Au donor and $G2$ DLTS peaks at depths between 1.1 and 1.6 μm . The sample contained approximately $5 \times 10^{14} \text{ cm}^{-3}$ hydrogen atoms within this depth region.

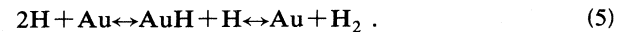
TABLE II. Reaction kinetics of association and dissociation of $G2$ at low temperatures. The data from Fig. 9 were fitted to the expression $k = k_0 \exp[-\Delta E/k_B T]$, where ΔE is an activation energy and k_0 is the prefactor.

Transition	k_0 (s^{-1})	ΔE (eV)
$G2 \rightarrow Au, k_D$	$2 \times 10^{9 \pm 1}$	1.02 ± 0.05
$Au \rightarrow G2, k_A$	$4 \times 10^{13 \pm 1}$	1.37 ± 0.05

where k_1 and k_2 are the rate constants of the association and the dissociation reactions and $[H]$, $[Au]$, and $[AuH]$ are the concentrations of each species. The dissociation rate of $G2$ in hydrogen-free surroundings is then determined by the second term in (3). However, Eq. (3) cannot explain the experimental observation that the dissociation of $G2$ is enhanced when excess hydrogen is present. There must be another competing reaction occurring at the same time that is not accounted for in Eq. (3). The simplest approach is to consider a competing reaction



i.e., hydrogen interacting with the Au-H complex, resulting in its dissociation with the hydrogen being released either as H_2 molecules, as suggested in Eq. (4), or as two separate H atoms. The overall reaction is then



If we assume that all the reactions are first order in each of the reactants, the rate equation for changes in AuH is

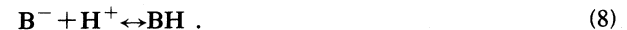
$$d[AuH]/dt = k_1[H][Au] - k_2[AuH] + k_3[H_2][Au] - k_4[H][AuH], \quad (6)$$

where k_3 and k_4 are the rate constants of the reverse and forward reactions in (4).

In addition to the reactions above, the formation of molecular hydrogen and reactions between boron and hydrogen have to be considered, i.e.,



and



The reactions described by Eqs. (7) and (8) were studied in great detail by Zundel and Weber.^{29,30} They concluded that the reactivation of boron acceptors was limited by reaction (7), i.e., atomic hydrogen was mainly lost as stable molecular hydrogen rather than by diffusion out of the sample region under investigation. In our case, during the annealing at low temperatures depicted in Fig. 5, no change in the active boron density is observed. Still the reverse bias annealing treatment at the end of the experiment revealed that the B-H density was approximately $5 \times 10^{14} \text{ cm}^{-3}$ in the region monitored with DLTS (see Sec. III D). This indicates that negligible hydrogen is lost through reaction (7) or through outdiffusion. This also agrees with the observation that the changes of the concentrations of $G2$ complexes, which depend on the concentration of atomic hydrogen, were fully reversible dur-

ing annealing between 75 and 130 °C. Therefore, as a first approximation, we neglect outdiffusion of hydrogen, as well as reaction (7). Further we assume that the H₂ density is small and neglect the third term in Eq. (6).

It should be noted that atomic hydrogen is lost as molecular hydrogen if the forward reaction in Eq. (4) occurs. This means that the reversibility depicted in Fig. 5 should be terminated. However, the hydrogen consumed in this manner would be only a small part of the atomic hydrogen stored in B-H pairs ($5 \times 10^{14} \text{ cm}^{-3}$). Such a change is within experimental error when determining the association and dissociation rates shown in Fig. 9.

The annealing data of G2 when no free H is present (Fig. 4) show that the dissociation rate k_2 is low at these temperatures, and we neglect the second term in Eq. (6). Using the approximations above, Eq. (6) becomes

$$d[\text{AuH}]/dt \approx k_1[\text{H}][\text{Au}] - k_4[\text{H}][\text{AuH}]. \quad (9)$$

We assume further that dynamical equilibrium ($d[\text{BH}]/dt \approx 0$) is achieved for reaction (8) at each temperature. This was the case in the work of Zundel and

Weber,³⁰ who used comparable annealing times and temperatures as in the present study to examine hydrogen diffusion. This means that at each temperature we have the following relation between the density of hydrogen and B-H complexes:³⁰

$$[\text{BH}] \approx (\sigma N_A / \nu)[\text{H}]. \quad (10)$$

Here σ is the capture rate for hydrogen at a boron acceptor, N_A is the boron acceptor concentration, and ν is the dissociation rate of the B-H complex.²⁶ Further, Zundel and Weber³⁰ concluded that most of the hydrogen was stored in B-H pairs during annealing at these temperatures, i.e., $[\text{BH}] \gg [\text{H}]$. The total concentration of atomic hydrogen is then $[\text{H}]_T = [\text{BH}] + [\text{H}] \approx [\text{BH}]$.

The capture rate of hydrogen at a boron acceptor is given by $\sigma = 4\pi D_i R_B$, where D_i is the diffusion coefficient of hydrogen and R_B is the capture radius of hydrogen at a boron site. If we use a similar approach³¹ for trapping of a hydrogen atom at a gold site, the rate constant k_1 can be written as $k_1 = 4\pi D_i R_{\text{Au}}$. Inserting this into (9), and making use of Eq. (10) together with the expression for the dissociation rate of the B-H complex²⁶ $\nu = \nu_0 \exp[-\Delta E_{\text{BH}}/k_B T]$, we obtain

$$d[\text{AuH}]/dt \approx (R_{\text{Au}}/R_B)(\nu_0/N_A) \exp(-\Delta E_{\text{BH}}/k_B T)[\text{H}]_T[\text{Au}] - (k_4/R_B)(\nu_0/4\pi D_i N_A) \exp(-\Delta E_{\text{BH}}/k_B T)[\text{H}]_T[\text{AuH}]. \quad (11)$$

The capture radius for hydrogen at a gold site (R_{Au}) can be expected to be of the order of the interatomic spacing³² if no Coulomb or other long-range forces are involved. If a possible temperature dependence of R_{Au} is neglected, the first term in Eq. (11) has an activation energy of $\approx \Delta E_{\text{BH}} = 1.28 \text{ eV}$. Using $R_{\text{Au}} = 2 \text{ \AA}$, $[\text{H}]_T = 5 \times 10^{14} \text{ cm}^{-3}$, and $N_A = 3 \times 10^{15} \text{ cm}^{-3}$, and the values for B-H pairs from Zundel and Weber³⁰ $\nu_0 = 2.8 \times 10^{14} \text{ s}^{-1}$ and $R_B = 35 \text{ \AA}$, the prefactor of the first term in (11) becomes $3 \times 10^{12} \text{ s}^{-1}$. This is in fair agreement with the data for k_A in Table II, $\Delta E = 1.37 \pm 0.04 \text{ eV}$, and a prefactor of $4 \times 10^{13 \pm 1} \text{ s}^{-1}$. This suggests that the formation of G2 at low temperatures is limited by the dissociation of B-H pairs.

If the dissociation energy of B-H pairs ($\Delta E = 1.28 \text{ eV}$) and the migration energy for hydrogen diffusion ($\Delta E_m = 0.48 \text{ eV}$) (Ref. 33) are inserted into Eq. (11) the second term has an activation energy of about 0.8 eV plus a possible activation energy of the rate constant k_4 . For comparison, the rate constant k_D in Table II has an activation energy of 1.02 eV. Provided that the reaction in Eq. (4) correctly describes the dissociation of G2, this means that the activation energy for the forward reaction in (4) is small.

The reactions discussed above are one alternative explanation of the dissociation and association of G2 at low temperatures. Since so many different reactions, structural and electronic, seem to be involved, our approach should be considered as a first approximation. Still, it should be pointed out that reactions analogous to

(2) and (4) have been used to describe passivation and depassivation of P_b centers by hydrogen at the SiO₂/Si interface.^{34,35} In addition, a reaction similar to (4) has been studied theoretically for the interaction between boron and hydrogen, and phosphorus and hydrogen, in silicon. However, the result of that study was that B-H₂ and P-H₂ would form instead of dissociation of B-H and P-H and simultaneous formation of H₂.³⁶

We now turn to the conversion of G2 into PA complexes at 150 °C (Fig. 3). As mentioned above, additional hydrogen is apparently needed for this process to occur. We tentatively assigned G2 to Au-H and PA to Au-H₂. This suggests the reaction



This process would then compete with reaction (4). Experimentally at 150 °C we only observe conversion of G2 into PA, so reaction (12) appears to dominate at higher temperatures ($T \geq 150 \text{ °C}$) while reaction (4) is the main process at lower temperatures. Conversion of gold donors into passive gold hydrogen complexes (PA) was also observed at 150 °C if free hydrogen was present (Fig. 3). It is not clear if this gold passivation occurs via reactions (2) and (12) or in a single step ($\text{Au} + 2\text{H} \rightarrow \text{AuH}_2$). The data in Fig. 3(a) suggest that some of the gold donors directly form passive Au-H complexes, and that this process requires more hydrogen than the G2-to-PA conversion. The data on *n*-type samples also support this picture (Fig. 8). Still, more data are needed if all the reactions suggested above are to be properly distinguished.

B. Connection between DLTS peaks in *p*- and *n*-type samples

In *n*-type samples we observed a decrease in the *G*1 concentration during annealing at 150°C. The *G*1 concentration decreased at first but became constant after about an hour as shown in Fig. 8(c). The Au+*G*4 concentration showed the same behavior. We explain this as a transformation of the active Au-H complex, detected as *G*1 and *G*4, into a passive Au-H complex. This is qualitatively similar to what happened in *p*-type samples, where *G*2 transformed into PA at 150°C if free hydrogen was present as shown in Fig. 3(a). Also, there is a correlation between the occurrence of *G*2 and *G*4 in *p*-type samples as shown in Fig. 6 and between *G*1 and *G*4 in *n*-type samples (see Fig. 8). Together this suggests that all three levels belong to the same center, which we label *G*.

The deep levels of gold are shown in Fig. 10 along with the *G* levels. One way of looking at the *G* levels is to explain them qualitatively as shifts in the deep levels of gold, as indicated in the figure. In such terms, the gold donor level is shifted about 0.13 eV. The gold acceptor level is not significantly shifted, but the electron and hole emission rates are altered. The *G*1 level is then possibly due to a downward shift of Au^{-/-}. The second acceptor level of gold has not been observed experimentally. If it exists at all it is probably located close to or in the conduction band. If the *G* center is amphoteric, *G*1 is expected to be its second acceptor level, *G*4 the first acceptor level, and *G*2 the first donor level. Previous studies of highly gold-doped samples revealed that *G*1 centers compensate phosphorus donors, and it was concluded that *G*1 is an acceptor level.¹⁴ The electron-capture cross section of *G*1 is also small (1×10^{-17} cm²), as expected for a double acceptor level. Similar attempts to clarify the donor or acceptor character of *G*2 have not been conclusive. The passive Au-H complex PA has no deep levels within the band gap. Still it is possible that PA has a shallow level or levels that is (are) inaccessible with DLTS.

Since the *G* levels are readily formed after wet etching of gold-doped silicon, these levels should have been observed in previous studies of gold-doped Schottky diodes. In *n*-type silicon an unidentified level similar to the *G*1 level is frequently observed (see Ref. 14 and references therein). Deep levels with depth distributions and thermal stability similar to those of *G*2 and *G*3 have been reported by Lemke.³⁷ Figure 11 is an Arrhenius plot of

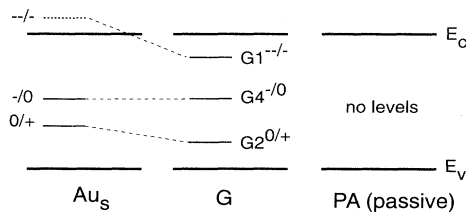


FIG. 10. Deep levels of gold and the hydrogen-gold complex labeled *G*. The second acceptor level of gold has not been observed experimentally. If it exists at all it is probably located close to or in the conduction band. The charge state assignment of the *G* levels is only tentative.

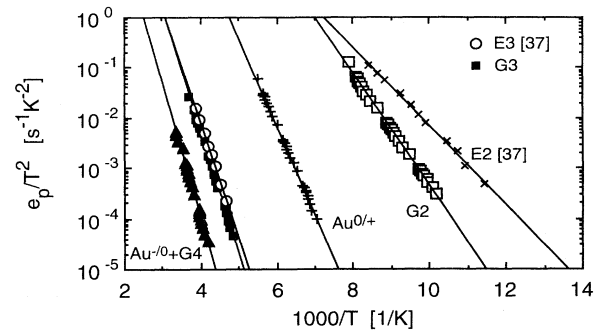


FIG. 11. Arrhenius plot of the hole emission rates of the deep levels in *p*-type samples. The hole emission from *G*2 and *G*3 is compared with data of Lemke (Ref. 37) on levels (*E*2 and *E*3) observed in gold-doped silicon.

the hole emission rates of the levels in *p*-type samples. The hole emission rates of *G*2 and *G*3 can be compared to those of levels *E*2 and *E*3 of Lemke.³⁸ The data for *G*3 and *E*3 are almost identical, while there is a considerable difference between the data for *G*2 and *E*2.

C. Formation of Au-H complexes in *p*- and *n*-Si

The role of the charge states of gold and hydrogen during complex formation is not clear. Indeed the complex formation seems to depend mostly on the interaction between hydrogen and the shallow dopants in the samples. Gold acceptors in *n*-Si are strongly passivated in the surface region after etching, but gold donors in *p*-Si are not. In *p*-Si most of the incoming hydrogen immediately forms pairs with boron, while in *n*-type samples only a portion of the hydrogen forms pairs with phosphorus. Apparently, in *p*-Si the hydrogen must first be released from B-H pairs to be able to form the passive Au-H₂ complex (PA). This increases the activation energy of formation of PA as compared to *n*-Si by roughly ≈ 0.8 eV (i.e., $\Delta E_{BH} - \Delta E_m$). In *n*-Si a considerable part of the hydrogen is free, which already enables the formation of PA at room temperature. Also, the passive complex appears to be favored in regions with high hydrogen density. PA is favored closest to the surface in *n*-type samples where the hydrogen density is largest, while the active complex (Au-H), observed as *G*1 (and *G*4), dominates deeper in the sample.

The charge state of gold is known from the location of its deep levels, but the charge state of hydrogen is less clear. The donor level of isolated hydrogen at $E_c - 0.16$ eV is rather well established,⁴⁻⁶ while the location (or even existence) of the acceptor level is uncertain. Recent experimental findings suggest that the acceptor level is close to midgap.⁷ In *p*-Si hydrogen is expected to be predominantly positively charged under all circumstances.^{2,26} It seems as if the *G* levels are formed without the need of a Coulomb interaction. The *G*2 level appears even when both species are positively charged, Au⁺ and H⁺. The expected repulsive force between the two species could influence the activation energies for the transition between gold donors and *G*2 that were discussed in Sec. IV A.

D. Gold passivation: Comparison with previous studies

The results of the first study of passivation of gold by hydrogen²² differ considerably from the results of the present work. First of all, no additional deep levels were reported after hydrogenation, only passivation of the deep levels of gold. Gold was then partially reactivated by annealing at 400 °C. In this work, three deep levels ($G1$, $G2$, and $G4$) are observed after hydrogen injection at the same time as a portion of the gold centers are passivated. Also, it is sufficient to anneal the samples for 60 min at 250 °C to dissociate the Au-H complexes almost fully. The thermal stability of the gold passivation seems to be weaker in this work than in the previous study,²² but the annealing kinetics of the reactivation have not yet been properly studied.

However, the experimental conditions are different. We introduced low doses of hydrogen, typically about 10^{15} atoms/cm³, into the sample surface region by etching at room temperature. In the work of Pearton and Tavendale²² the samples were annealed at temperatures between 150 and 350 °C in hydrogen plasma. These temperatures might prevent the formation of the electrically active Au-H complexes observed by us. Also, the hydrogen concentration in their samples is evidently much higher than in our samples, so the passive Au-H complex is expected to dominate in their samples. This agrees with a study of Pearton and Tavendale, where low doses of hydrogen were introduced into gold-doped silicon by boiling in water. Such treatment resulted in formation of deep levels that were not investigated further.³⁸

V. CONCLUSIONS

In summary, we conclude that gold and hydrogen form two separate complexes. The complex G is electrically active while the complex PA is electrically inactive. G transforms irreversibly into PA during annealing. From the kinetics of the reaction we propose that the complexes contain different numbers of hydrogen atoms. We suggest that the G complex is a Au-H pair, while the passive complex is Au-H₂. The annealing kinetics of G in p -type samples are unusual in the sense that the complex dissociates faster if atomic hydrogen is present in the surroundings. We qualitatively explain this by the reaction $H + AuH \rightarrow Au + H_2$. The formation and annealing of the Au-H complexes in p -type silicon are strongly influenced by association and dissociation of B-H pairs which control the concentration of excess hydrogen atoms. The passive complex (Au-H₂) seems to dominate in hydrogen-rich regions of the samples, while the active complex (Au-H) is detected in regions with lower hydrogen density. This is a possible explanation of the absence of the active Au-H complex in previous studies, where high doses of hydrogen were introduced into gold-doped silicon by remote plasma.²²

ACKNOWLEDGMENTS

We thank Per Ericsson for helpful discussions. This work was financially supported by the Swedish National Board for Industrial and Technical Development (NUTEK).

- ¹J. I. Pankove and N. M. Johnson, in *Hydrogen in Semiconductors*, edited by J. I. Pankove and N. M. Johnson, Semiconductors and Semimetals Vol. 34 (Academic, San Diego, 1991), pp. 1–15.
- ²S. J. Pearton, J. W. Corbett and M. Stavola, *Hydrogen in Crystalline Semiconductors* (Springer, Berlin, 1992).
- ³C. H. Seager, in *Hydrogen in Semiconductors* (Ref. 1), pp. 17–33.
- ⁴B. Holm, K. Bonde Nielsen, and B. Bech Nielsen, *Phys. Rev. Lett.* **66**, 2360 (1991).
- ⁵B. Bech Nielsen, K. Bonde Nielsen, and J. R. Byberg, *Mater. Sci. Forum* **143-147**, 909 (1994).
- ⁶N. M. Johnson and C. Herring, *Mater. Sci. Forum* **143-147**, 867 (1994).
- ⁷N. M. Johnson, C. Herring, and C. G. Van de Walle, *Phys. Rev. Lett.* **73**, 130 (1994).
- ⁸S. J. Pearton, in *Hydrogen in Semiconductors* (Ref. 1), pp. 65–89.
- ⁹I. A. Veloriso, M. Stavola, D. M. Kozuch, R. E. Peale, and G. D. Watkins, *Appl. Phys. Lett.* **59**, 2121 (1991).
- ¹⁰S. A. McQuaid, R. C. Newman, J. H. Tucker, E. C. Lightowers, R. A. A. Kubiak, and M. Goulding, *Appl. Phys. Lett.* **58**, 2933 (1991).
- ¹¹P. M. Williams, G. D. Watkins, S. Uftring, and M. Stavola, *Phys. Rev. Lett.* **70**, 3816 (1993); *Mater. Sci. Forum* **143-147**, 891 (1994).
- ¹²M. Höhne, U. Juda, Y. V. Martynov, T. Gregorkiewicz, C. A. J. Ammerlaan, and L. S. Vlasenko, *Phys. Rev. B* **49**, 13 423 (1994).
- ¹³S. J. Pearton and E. E. Haller, *J. Appl. Phys.* **54**, 3613 (1983).
- ¹⁴E. Ö. Sveinbjörnsson and O. Engström, in *Defect Engineering in Semiconductor Growth, Processing and Device Technology*, edited by S. Ashok, J. Chevallier, K. Sumino, and E. Weber, MRS Symposia Proceedings No. 262 (Materials Research Society, Pittsburgh, 1992), p. 501; *Appl. Phys. Lett.* **61**, 2323 (1992).
- ¹⁵T. Sadoh, H. Nakashima, and T. Tsurushima, *J. Appl. Phys.* **72**, 520 (1992).
- ¹⁶E. Ö. Sveinbjörnsson, G. I. Andersson, and O. Engström, *Phys. Rev. B* **49**, 7801 (1994).
- ¹⁷E. Ö. Sveinbjörnsson and O. Engström, *Mater. Sci. Forum* **143-147**, 821 (1994).
- ¹⁸T. Sadoh, M. Watanabe, H. Nakashima, and T. Tsurushima, *J. Appl. Phys.* **75**, 3978 (1994).
- ¹⁹H. Feichtinger and E. Sturm, *Mater. Sci. Forum* **143-147**, 111 (1994).
- ²⁰J. W. Petersen and J. Nielsen, *Appl. Phys. Lett.* **56**, 1122 (1990).
- ²¹G. D. Watkins, M. Kleverman, A. Thilderkvist, and H. G. Grimmeiss, *Phys. Rev. Lett.* **67**, 1149 (1991).
- ²²S. J. Pearton and A. J. Tavendale, *Phys. Rev. B* **26**, 7105 (1982).
- ²³E. Ö. Sveinbjörnsson, O. Engström, and U. Södervall, *J. Appl. Phys.* **73**, 7311 (1993).
- ²⁴G. I. Andersson and O. Engström, *J. Appl. Phys.* **67**, 3500 (1990).
- ²⁵D. V. Lang, *J. Appl. Phys.* **45**, 3023 (1974).
- ²⁶T. Zundel and J. Weber, *Phys. Rev. B* **39**, 13 549 (1989).

- ²⁷S. D. Brotherton, and J. E. Lowther, *Phys. Rev. Lett.* **44**, 606 (1980).
- ²⁸O. Engström and A. Alm, *Solid-State Electron.* **21**, 1571 (1978).
- ²⁹T. Zundel and J. Weber, *Phys. Rev. B* **43**, 4361 (1991).
- ³⁰T. Zundel and J. Weber *Phys. Rev. B* **46**, 2071 (1992).
- ³¹H. Reiss, C. S. Fuller, and F. J. Morin, *Bell. Syst. Tech. J.* **35**, 535 (1956).
- ³²C. Herring and N. M. Johnson, in *Hydrogen in Semiconductors* (Ref. 1), pp. 225–350.
- ³³A. Van Wieringen and N. Warmoltz, *Physica (Utrecht)* **22**, 849 (1956).
- ³⁴K. L. Brower, *Phys. Rev. B* **42**, 3444 (1990).
- ³⁵A. H. Edwards, *Phys. Rev. B* **44**, 1832 (1991).
- ³⁶L. Korpás, J. W. Corbett, and S. K. Estreicher, *Phys. Rev. B* **46**, 12 365 (1992).
- ³⁷H. Lemke, *Phys. Status Solidi A* **92**, K139 (1985).
- ³⁸S. J. Pearton (unpublished).